Journal of Solid State Chemistry 182 (2009) 1473–1480

Contents lists available at ScienceDirect

Journal of Solid State Chemistry

journal homepage: www.elsevier.com/locate/jssc

Nickel deficiency in $RENi_{2-x}P_2$ (RE = La, Ce, Pr). Combined crystallographic and physical property studies

Svilen Bobev [a,*], Sheng-qing Xia [a,1], Eric D. Bauer [b], Filip Ronning [b], Joe D. Thompson [b], John L. Sarrao [b]

[a] Department of Chemistry and Biochemistry, University of Delaware, Newark, DE 19716, USA
[b] Materials Physics and Applications Division (MPA-10), Los Alamos National Laboratory, Los Alamos, NM 87545, USA

ARTICLE INFO

Article history:
Received 8 December 2008
Received in revised form
25 February 2009
Accepted 21 March 2009
Available online 5 April 2009

Keywords:
$PrNi_2P_2$
$CeNi_2P_2$
Crystal structure
Single-crystal X-ray diffraction
Structural disorder

ABSTRACT

Large single crystals from $RENi_{2-x}P_2$ (RE = La, Ce, Pr) were synthesized from the pure elements using Sn as a metal flux, and their structures were established by X-ray crystallography. The title compounds were confirmed to crystallize in the body-centered tetragonal $ThCr_2Si_2$ structure type (space group $I4/mmm$ (No. 139); Pearson's symbol $tI10$), but with a significant homogeneity range with respect to the transition metal. Systematic synthetic work, coupled with accurate structure refinements indicated strong correlation between the degree of Ni-deficiency and the reaction conditions. According to the temperature dependent dc magnetization measurements, $LaNi_{2-x}P_2$ ($x = 0.30(1)$), as expected, is Pauli-like paramagnetic in the studied temperature regime, while the Ce-analog $CeNi_{2-x}P_2$ ($x = 0.28(1)$) shows the characteristics of a mixed valent Ce^{3+}/Ce^{4+} system with a possible Kondo temperature scale on the order of 1000 K. For three different $PrNi_{2-x}P_2$ ($x \leqslant 0.5$) samples, the temperature and field dependence of the magnetization indicated typical local moment $4f$-magnetism and a stable Pr^{3+} ground state, with subtle variations of T_C as a function of the concentration of Ni defects. Field-dependent heat capacity data for $CeNi_{2-x}P_2$ ($x = 0.28(1)$) and $PrNi_{2-x}P_2$ ($x = 0.53(1)$) are discussed as well.

1. Introduction

Ternary intermetallics with the general formula RM_2X_2, where R stands for the alkaline-earth and rare-earth metals, M is a transition metal and X denotes an early p-block element (groups 13–15), are ubiquitous and frequently investigated [1–30]. Among these, the most commonly encountered structures are the body-centered tetragonal $ThCr_2Si_2$ (Pearson's symbol $tI10$) and the trigonal $CaAl_2Si_2$ (Pearson's symbol $hP5$). Both atomic arrangements are relatively simple and are described by three crystallographically unique sites occupied by the three prototypical elements. Previous theoretical considerations for these structures, based on the density functional theory (DFT) and the extended Hückel method [5–10], have brought clear understanding of the similarities and the differences between their geometric and electronic requirements. The atomic site preferences in each case as a function of the electronegativity and size of the constituent elements are also established [5–10]. Therefore, it is not surprising that these two structure types are widely known as excellent candidates for rational tuning of a property of interest by substitutions of elements on specific sites. Examples of this approach abound [2,18–25], including several case studies from our laboratory [26–30].

As part of our continuing efforts to better understand the structure–property relationships in Zintl phases and intermetallics, we turned our attention to the chemical bonding and physical properties of various $R_xT_yPn_z$ ternary compounds, where Pn = pnicogen, i.e., group 15 element. These investigations were inspired by the very recent discovery of superconductivity in K-doped $BaFe_2As_2$ (long known compound with the $ThCr_2Si_2$ type) [22–25] and in a range of oxi-pnictides with the related ZrCuSiAs type [31]. Although, as noted above, a considerable amount of work on ternary pnictides has already been done, there are still many gaps and inconsistencies in the literature. For example, the existence of the $RENi_2P_2$ (RE = La, Ce, Pr) compounds was first reported in 1980 by Jeitschko et al. [32]. They were initially recognized from their X-ray powder diffraction patterns only, but in 1984 [33], the structures of $RENi_2P_2$ (RE = La and Ce) were established by single-crystal work. Despite the high-quality crystallography in the latter study, a basic question regarding the structure remained open; namely—the nature of the "small deviations, about 5% from full occupancy of the Ni and P positions" [33]. The authors state that even though the "refined with partial occupancy positions are highly significant from the

* Corresponding author. Fax: +1 302 831 6335
E-mail address: bobev@udel.edu (S. Bobev).
[1] Present address: State Key Laboratory of Crystal Materials, Institute of Crystal Materials, Shandong University, Jinan 250100, China.

0022-4596/$ - see front matter © 2009 Elsevier Inc. All rights reserved.
doi:10.1016/j.jssc.2009.03.014

standpoint of error analysis, it is, however, difficult to assess the physical meaning of this result" [33], and that "the ideal formulas $LaNi_2P_2$ and $CeNi_2P_2$ are well within the homogeneity ranges of the compounds" [33]. The results presented in this article address this issue and confirm that non-stoichiometry among the early rare-earth metal nickel phosphides with the $ThCr_2Si_2$ type, as suggested in earlier computational papers [5–9], is an inherent characteristics of the structure. Our syntheses and structure refinements, together with the property measurements, suggest a wide phase width in $RENi_{2-x}P_2$ (RE = La, Ce, Pr), which is strongly dependent on the reaction conditions. These findings underscore the importance of the careful synthetic and structural work, regardless of the apparent simplicity of the targeted phases.

2. Experimental

2.1. Synthesis

Handling of the starting materials (pure La, Ce and Pr from Ames Laboratory, Ni and red P from Alfa, used as received) was carried out inside an argon-filled glove box or under vacuum. In a typical experiment, a mixture of the elements with the desired stoichiometric ratio (total weight ca. 500 mg) was loaded in a 2 cm^3 alumina crucible, which was then topped off with 2–2.5 g Sn (Alfa, shots). This ensures 10–15 fold excess of Sn (with respect to the rare-earth metal) as a flux. The crucible was enclosed in a fused silica tube, which was then flame-sealed under vacuum. The evacuated ampoule with the mixture inside was heated in a programmable muffle-furnace to temperatures 1173–1423 K at rates of 50–200 °/h, allowed to homogenize for 4–8 h, followed by a slow cooling to 873 K at rates of 3–5 °/h. The flux was subsequently removed by centrifugation; further details on the procedure can be found elsewhere [34].

Several synthetic details of specific importance to the reaction outcome and ultimately, the physical properties, need to be explicitly mentioned here.

(1) Reactions with nominal composition RE:Ni:P = 1:2:2 carried out at lower temperatures (1173–1273 K) yielded $RENi_{2-x}P_2$ (RE = La, Ce, Pr) with a modest concentration of Ni defects ($x \approx 0$–0.1). The crystals obtained by such reactions were usually very small and often inapt for single-crystal X-ray diffraction studies.

(2) Reactions with the same nominal composition, but run at higher temperature (1423 K), yielded $RENi_{2-x}P_2$ (RE = La, Ce, Pr) with a higher degree of non-stoichiometry ($x \approx 0.25$). The outcomes of such reactions tended to be larger, plate-like single-crystals, together with small amounts of binary side products—Ni_2P, NiP_2, Ni_3Sn_4, Sn_3P_4, etc. [1].

(3) Reactions with nominal composition RE:Ni:P = 1:1:2 afforded the most Ni-deficient $RENi_{2-x}P_2$ (RE = La, Ce, Pr) samples. This is evidenced from the discussed below structure refinements of $PrNi_{2-x}P_2$ ($x = 0.53(1)$). These findings, together with the solubility issue mentioned below, confirm that the homogeneity range is a function of both the composition and the reaction temperature, suggesting that the cell volume variations detailed in Table 1 cannot be explained on the basis of possible polymorphic transitions.

(4) Reactions with nominal composition RE:Ni:P = 1:2:2, where Ni was cut from a large rod and not finely divided into smaller pieces yielded $RENi_{2-x}P_2$ (RE = La, Ce, Pr) with higher degree of non-stoichiometry and larger than expected amounts of Ni_3Sn_4. Such observation, although somewhat puzzling, is not difficult to comprehend—without any means to homogenize the mixture at the reaction temperature, there appear to be regions, in close proximity to the Ni piece, where the nucleation and crystal growth of the Ni-binary is facilitated, thereby leading to a depletion of the transition metal.

(5) $RENi_{2-x}P_2$ (RE = La, Ce, Pr) in single-crystalline form are stable in air and do not appear to lose their metallic luster over long periods of time. They can be etched with diluted solution of HCl (a means to clean the surfaces prior to property measurements).

2.2. Crystallographic Studies

X-ray powder diffraction patterns were taken at room temperature on a Rigaku MiniFlex powder diffractometer using Cu$K\alpha$ radiation (θ–θ scan mode with a step-size of 0.05° and rates of 3–5 s/step). The diffractograms were primarily used to assess the phase purity, an analysis that was carried out using the JADE 6.5 package [35]. The observed peak-positions and the peaks' relative intensities matched well with those calculated from the single-crystal work. Indexing of the patterns confirmed the reflection conditions expected for the body-centered tetragonal symmetry (Supporting Information). The powder XRD data with

Table 1
Unit cell constants for the ternary $RENi_{2-x}P_2$ (RE = La, Ce, Pr) compounds, synthesized using different conditions.

Compound ($ThCr_2Si_2$ type)	Unit cell parameters				Reference	Synthesis method
	a (Å)	c (Å)	c/a	V (Å^3)		
$LaNi_2P_2$	4.007(2)	9.632(6)	2.404	154.6	[32]	1043 K—Sn flux
$LaNi_2P_2$[a]	4.010(1)	9.604(2)	2.395	154.4	[33]	1173 K—Sn flux
$LaNi_{1.70(1)}P_2$[b]	*4.018(2)*	*9.485(6)*	*2.361*	*153.1*	*this work*	*1423 K—Sn flux*
$CeNi_2P_2$	3.955(2)	9.505(6)	2.403	148.7	[32]	1043 K—Sn flux
$CeNi_2P_2$[a]	3.958(1)	9.489(2)	2.397	148.7	[33]	1173 K—Sn flux
$CeNi_{1.88(2)}P_2$[b]	*3.956(2)*	*9.489(3)*	*2.398*	*148.5*	*this work*	*1173 K—Sn flux*
$CeNi_{1.72(1)}P_2$[b]	*3.960(1)*	*9.416(1)*	*2.377*	*147.6*	*this work*	*1423 K—Sn flux*
$PrNi_2P_2$	3.952(2)	9.493(6)	2.402	148.3	[32]	1043 K—Sn flux
$PrNi_{1.97(2)}P_2$[b]	*3.956(2)*	*9.489(6)*	*2.399*	*148.5*	*this work*	*1173 K—Sn flux*
$PrNi_{1.89(1)}P_2$[b]	*3.957(1)*	*9.485(3)*	*2.395*	*148.5*	*this work*	*1273 K—Sn flux*
$PrNi_{1.47(1)}P_2$[b]	*3.968(1)*	*9.269(1)*	*2.336*	*145.9*	*this work*	*1423 K—Sn flux, substoichiometric Ni*

Data from this study are italicized. Cell parameters from this work were determined by powder X-ray diffraction with Si as an internal standard (Cu$K\alpha$, room temperature).
[a] Single-crystal refinements reportedly indicate small deviations, ca. 5%, from full occupancy on both the Ni and P positions.
[b] Nickel deficiency determined from single-crystal refinements—Table 2.

Table 2
Selected single-crystal data collection and structure refinement parameters for $RENi_{2-x}P_2$ (RE = La, Ce, Pr).

Empirical formula	$LaNi_{1.70(1)}P_2$	$CeNi_{1.88(2)}P_2$	$CeNi_{1.72(1)}P_2$	$PrNi_{1.97(2)}P_2$	$PrNi_{1.89(1)}P_2$	$PrNi_{1.47(1)}P_2$
Formula weight, $Z=2$	300.66	312.43	304.8	318.51	315.57	289.15
Crystal system	Tetragonal					
Space group	I4/*mmm*, No. 139					
Temperature	120 K					
Unit cell dimensions (Å)	$a=4.0175(4)$	$a=3.9535(10)$	$a=3.9440(2)$	$a=3.951(1)$	$a=3.9531(4)$	$a=3.9599(8)$
	$c=9.454(2)$	$c=9.468(5)$	$c=9.3737(10)$	$c=9.466(6)$	$c=9.462(2)$	$c=9.246(4)$
Volume (Å^3)	152.59(4)	147.98(9)	145.81(2)	147.8(1)	147.87(4)	144.98(7)
Density (calculated, g/cm^3)	6.544	7.012	6.942	7.161	7.088	6.624
Radiation	Mo$K\alpha$, $\lambda=0.71073$ Å					
Absorption coefficient (cm^{-1})	248.9	277.2	273.2	294.1	290.7	268.1
Data/restraints /parameters	76/0/10					
R indices ($I>2\sigma_I$)[a]	$R1=0.0154$	$R1=0.0259$	$R1=0.0188$	$R1=0.0309$	$R1=0.0115$	$R1=0.0273$
	$wR2=0.0328$	$wR2=0.0606$	$wR2=0.0424$	$wR2=0.0608$	$wR2=0.0256$	$wR2=0.0584$
R indices (all data)[a]	$R1=0.0173$	$R1=0.0291$	$R1=0.0188$	$R1=0.0343$	$R1=0.0118$	$R1=0.0302$
	$wR2=0.0334$	$wR2=0.0615$	$wR2=0.0424$	$wR2=0.0621$	$wR2=0.0257$	$wR2=0.0591$
Goodness-of-fit on F^2	1.218	1.114	1.164	1.188	1.111	1.210
Largest diff. peak/hole (e/Å^3)	1.456/–0.692	1.820/–1.015	1.121/–1.117	1.449/–1.657	0.542/–0.438	1.242/–1.037

[a] $R1=\sum||F_o|-|F_c||/\sum|F_o|$; $wR2=[\sum[w(F_0^2-F_c^2)^2]/\sum[w(F_0^2)^2]]^{1/2}$, where $w=1/[\sigma^2F_0^2+(A\cdot P)^2+B\cdot P]$, and $P=(F_0^2+2F_c^2)/3$; A and B—weight coefficients.

silicon added as an internal standard also allowed for the least-squares refinements of the unit cell parameters. This information is provided in Table 1 for all synthesized samples.

Single-crystal X-ray diffraction data were collected using a Bruker SMART CCD-based diffractometer (3-cirlce goniometer, Mo$K\alpha$ source). All data collections were carried out in batch runs at different ω and ϕ angles. Suitable crystals from the synthesized were selected under a microscope and cut to ca. 0.04–0.07 mm in all dimensions. Many crystals were tried and checked for singularity before picking the best ones. The typical data-collection (done at 120 K) involved 0.5°-scans in ω with 10–15 s per frame exposure and was carried out using the SMART software [36]. Data integration and global unit cell refinement were done using SAINT, respectively [36]. SADABS was used for semi-empirical absorption correction based on equivalents [37].

In all analyzed cases, the systematic absence conditions $h+k+l=2n$ confirmed the body-centered Bravais class. This validated the previous reports [33] and indicated that the tetragonal $ThCr_2Si_2$ type with space group *I4/mmm* (No. 139) [1] is the most likely choice of a starting model for refinements. The structure was subsequently refined by full matrix least-squares methods on F^2 using SHELXL [38]. Although the refinement cycles proceeded smoothly, in some cases, large displacement parameters, poor convergence, and relatively high residuals for such a simple structure were noted. To diagnose these problems, refinements of the site occupation factors were undertaken (done by freeing the site occupancy of an individual site, while the remaining occupation parameters were kept fixed). This resulted in statistically insignificant deviations from unity for the rare-earth metal and the phosphorus sites, but the Ni sites were consistently underoccupied, in some case by more than 25%. Such findings are consistent with earlier work on isotypic nickel phosphides such as $UNi_{2-x}P_2$ [16] and $CaNi_{2-x}P_2$ [39], and confirmed by the EDX analysis and the variations of the unit cell constants (Table 1). The possibility to resolve the disorder by finding larger translation periods and/or lower symmetry space groups (e.g., $I\bar{4}m2$ or even re-integration of the raw data in attempts to use $CaBe_2Ge_2$ type [1] as a model) were unsuccessful. We note here that although our intensity data (in-house X-ray system) did show evidence for a superstructure, synchrotron or electron diffraction could help identify possible long-range ordered structure. Further details of the data collection and structure refinements parameters for six representative data sets are given in Table 2. In the final refinement cycles, the three atomic positions were refined with anisotropic displacement parameters and freed occupancy for the Ni site. Final positional and equivalent isotropic displacement parameters and important bond distances are listed in Tables 3 and 4, respectively. Additional information in the form of CIF has been deposited with Fachinformations-zentrum Karlsruhe, 76344 Eggenstein-Leopoldshafen, Germany—depository numbers CSD 420100 ($LaNi_{1.70(1)}P_2$); CSD 380283 ($CeNi_{1.88(1)}P_2$); CSD 420101 ($CeNi_{1.72(1)}P_2$); CSD 380284 ($PrNi_{1.97(1)}P_2$); CSD 420102 ($PrNi_{1.89(1)}P_2$); and CSD 420103 ($PrNi_{1.47(1)}P_2$).

Table 3
Refined atomic coordinates and equivalent isotropic displacement parameters for $RENi_{2-x}P_2$ (RE = La, Ce, Pr).

Atom	Wyckoff site	x	y	Z	U_{eq} (Å^2)	Occup.
$LaNi_{1.70(1)}P_2$						
La	2*a*	0	0	0	0.013(1)	1.00
Ni	4*d*	0	1/2	1/4	0.010(1)	0.853(6)
P	4*e*	0	0	0.3716(2)	0.009(1)	1.00
$CeNi_{1.88(2)}P_2$						
Ce	2*a*	0	0	0	0.007(1)	1.00
Ni	4*d*	0	1/2	1/4	0.008(1)	0.936(9)
P	4*e*	0	0	0.3735(4)	0.009(1)	1.00
$CeNi_{1.72(1)}P_2$						
Ce	2*a*	0	0	0	0.009(1)	1.00
Ni	4*d*	0	1/2	1/4	0.008(1)	0.861(4)
P	4*e*	0	0	0.3742(2)	0.008(1)	1.00
$PrNi_{1.97(2)}P_2$						
Pr	2*a*	0	0	0	0.007(1)	1.00
Ni	4*d*	0	1/2	1/4	0.009(1)	0.98(1)
P	4*e*	0	0	0.3733(5)	0.007(1)	1.00
$PrNi_{1.89(1)}P_2$						
Pr	2*a*	0	0	0	0.008(1)	1.00
Ni	4*d*	0	1/2	1/4	0.008(1)	0.946(4)
P	4*e*	0	0	0.3737(2)	0.008(1)	1.00
$PrNi_{1.47(1)}P_2$						
Pr	2*a*	0	0	0	0.017(1)	1.00
Ni	4*d*	0	1/2	1/4	0.009(1)	0.735(7)
P	4*e*	0	0	0.3752(3)	0.008(1)	1.00

2.3. EDX Analysis

To corroborate the structure refinements, particularly for the $PrNi_{1.47(1)}P_2$ sample, where the Ni-deficiency is most pronounced,

Table 4
Selected bond distances (Å) for $RENi_{2-x}P_2$ (RE = La, Ce, Pr).

$LaNi_{1.70(1)}P_2$		$CeNi_{1.88(2)}P_2$		$CeNi_{1.72(1)}P_2$	
Ni–P	2.314(1) × 4	Ni–P	2.297(2) × 4	Ni–P	2.2899(8) × 4
Ni–Ni	2.841(1) × 4	Ni–Ni	2.7955(7) × 4	Ni–Ni	2.7888(1) × 4
P–P	2.428(5)	P–P	2.395(9)	P–P	2.359(3)
La–P	3.089(1) × 8	Ce–P	3.041(2) × 8	Ce–P	3.0280(6) × 8
La–Ni	3.1018(4) × 4	Ce–Ni	3.084(1) × 4	Ce–Ni	3.0627(2) × 4
La–La	4.0175(4) × 4	Ce–Ce	3.9535(10) × 4	Ce–Ce	3.9440(2) × 4
$PrNi_{1.97(2)}P_2$		$PrNi_{1.89(1)}P_2$		$PrNi_{1.47(1)}P_2$	
Ni–P	2.294(3) × 4	Ni–P	2.2973(8) × 4	Ni–P	2.293(2) × 4
Ni–Ni	2.7934(9) × 4	Ni–Ni	2.7953(3) × 4	Ni–Ni	2.8001(1) × 4
P–P	2.399(10)	P–P	2.390(3)	P–P	2.309(8)
Pr–P	3.040(3) × 8	Pr–P	3.0399(7) × 8	Pr–P	3.029(2) × 8
Pr–Ni	3.083(1) × 4	Pr–Ni	3.0826(4) × 4	Pr–Ni	3.0435(7) × 4
Pr–Pr	3.951(1) × 4	Pr–Pr	3.9531(4) × 4	Pr–Pr	3.9599(8) × 4

single crystals from it were subjected to elemental micro-analysis. For the purpose, several plate-like crystals with clean surfaces were mounted onto carbon tape and brought inside the vacuum chamber of a Jeol 7400 F electron microscope. The instrument was equipped with an INCA-Oxford energy-dispersive spectrometer and was operated at 10 μA beam current at 15 kV accelerating potential. Many spots on the crystals' surface were analyzed, giving a ratio of Pr:Ni:P = 1:1.4:2.2 (atomic%, averaged from more than 10 data points). This ratio confirms the deviation from the ideal stoichiometry and agrees fairly well (within the error of the method) with the composition refined from the single-crystal X-ray diffraction data (Table 2). The analysis did not detect any other elements, besides traces of Sn flux.

2.4. Property measurements

Field-cooled *dc* magnetization measurements were performed in a Quantum Design MPMS-2 SQUID from 5 to 300 K in an applied magnetic field of 500 Oe. The samples (typically 10–20 mg) were secured in wax-paper, wrapped with a Kapton tape. Raw data were corrected for diamagnetic contribution from the holder and converted to molar magnetic susceptibility (units of emu/mol). Zero field-cooled measurements were performed from 5 to 50 K in an applied magnetic field of 100 Oe. Field-sweeps were performed at 5 K in applied field up to 50 kOe. All measurements were repeated for specimens from different batches in order to ensure reproducibility.

Specific heat $C_p(T)$ data were obtained on single-crystals using a custom-designed system. The thermal relaxation method in the temperature range 1.8–100 K was employed. Data were gathered without an external magnetic field and in applied fields of 30 and 90 kOe.

3. Results and discussion

3.1. Structure and bonding

Formerly known as the line compounds $RENi_2P_2$ [32,33], and reformulated herein as the Ni-deficient $RENi_{2-x}P_2$ (RE = La, Ce, Pr), crystallize with the $ThCr_2Si_2$ structure, a ternary variant of the $BaAl_4$ type—one of the most popular structure types among intermetallics [1]. Since this atomic arrangement is not without a precedent, only a brief account of the structure will be given here. For a more detailed description, we refer the reader to several comprehensive treatises on the $BaAl_4$ structure and its variants [2–10]. In the following discussions on the chemical bonding and

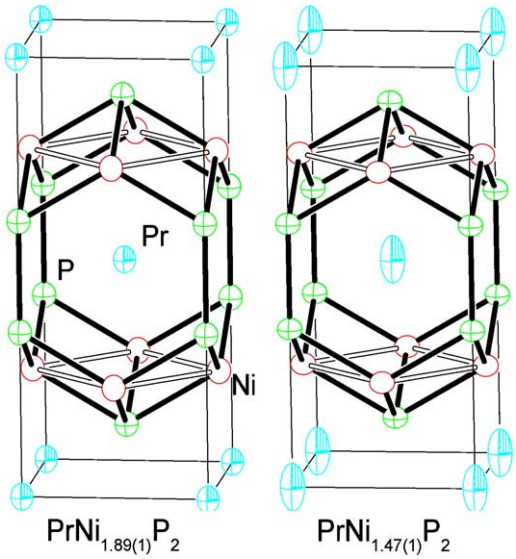

Fig. 1. Representations of the body-centered tetragonal structure of $PrNi_{1.89(1)}P_2$ and $PrNi_{1.47(1)}P_2$ ($ThCr_2Si_2$ type), viewed approximately along the [100] direction. The Ni–P polyanionic framework is emphasized; non-bonding Ni–Ni interactions are shown with open bonds. Anisotropic displacement parameters are drawn at the 95% probability level: Pr atoms are shown with full thermal ellipsoids, Ni atoms are represented with open circles and the P atoms are depicted with crossed ellipsoids. Unit cell is outlined. Online color code: Pr—blue, Ni—red, P—green. (For interpretation of references to colour in this figure legend, the reader is referred to the web version of this article.)

electronic structure, results from previous investigations on the fully stoichiometric $RENi_2P_2$ [5–10,32,33] will be used and further developed.

In the structure of $RENi_{2-x}P_2$, the La, Ce, and Pr cations (Wyckoff site 2*a*) are in a body-centered tetragonal arrangement (Fig. 1), with separation between them equal to the *a*-cell constant. The Ni atoms (Wyckoff site 4*d*, commonly referred to as a *basal* position) form square nets, which are capped from both sides in an alternating fashion by P (Wyckoff site 4*e*, the *apical* position). This bonding pattern results in two-dimensional slabs, in which, each Ni atom is nearly tetrahedrally coordinated by four P atoms, and each P atom is connected to four nearest Ni neighbors in a square pyramidal fashion, as depicted on Fig. 1. The P atoms from adjacent layers are close together at P–P distances ranging from 2.31 to 2.43 Å. This distance is particularly sensitive to the degree of Ni-deficiency and the size of the lanthanide metal (Table 4). Along these lines, another important observation, which deserves a special mention here, is the fact that higher concentration of vacant Ni sites apparently "disturbs" the equilibrium position of the rare-earth metal, residing at the center of an 18-vertex Fedorov polyhedron. This is clearly represented in Fig. 1, where the structures of $PrNi_{1.89(1)}P_2$ and $PrNi_{1.47(1)}P_2$ are represented side-by-side with anisotropic displacement parameters (ADP)—the elongation along the [001] direction of the ADP of the Pr atom in $PrNi_{1.47(1)}P_2$, compared to the normal ADP of the Pr atom in $PrNi_{1.89(1)}P_2$ is immediately seen. Notice that, this happens regardless of the largely uniaxial cell contraction (*c*-axis decreases by about 2.5%) caused by the Ni-defects. A simplistic geometric reasoning might explain this, taking into account the need for effective space-filling and the fact that two out of 8 next-nearest Ni atoms are missing. Changes in the electrostatic field around the rare-earth metal cation due to the missing Ni atoms can also be brought up as a possible explanation of the observed effect.

The P–P distances in all four refined structures are within the range or slightly longer than the expected for a single-bonded

pair, while the Ni–Ni contacts are on the order of 2.80 Å (Table 4), much longer than the Ni–Ni distances in elemental Ni, 2.49 Å [1]. This is consistent with the previously developed bonding picture for this structure [5–10], which can be rationalized in terms of five-center six-electron bonds within the layers and two-center two-electron bonds bridging them along the *c*-axis of the tetragonal unit cell. We draw attention to the fact that these contacts between two layers are a variable geometrical factor (expressed in the *c*/*a* ratio) and show a remarkable tunability—as discussed by Mewis [39], the series CaT_2P_2 for T = Fe, Co, Ni, Cu shows that the interlayer P–P decreases from 2.71–2.25 Å as the transition metal moves to the right-hand side in the Periodic Table. Taking these observations into account, Zheng and Hoffmann [5] carried out band structure calculations for a range of T_2X_2 frameworks, which clearly indicate an electronic effect at play here—the polyanionic sub-structure has an optimal count of 14 valence electrons per formula (N.B. only *s* and *p* electrons are considered here), and as *d*-bands get progressively filled on moving from left to right and their energy gets lowered, σ^*_{P-P} states are depopulated and the P–P separation, consequently, shortened [5]. More recent state-of-the-art DFT studies [9] provide a slightly different and more sophisticated interpretation, suggesting that strengthening the P–P interactions by filling the σ-bonding states at the top of the metal *d*-band should also be accompanied by weakening of the Ni–P interactions [9]. These computational results are supported by the variations of the unit cell parameters shown in Table 1—as the Ni-deficiency increases, Ni–P bonding weakens (*a* increases) and the interlayer P–P bonding strengthens (*c* decreases).

All of the above is well-known, therefore, it is surprising why the formation of Ni-defects in the discussed rare-earth metal nickel-phosphides has remained an overcast issue for such a long time. After all, defects at the transition metals sites are recognized in a number of isotypic compounds with late *d*-metals such as $CaNi_{2-x}P_2$ [39], $CaCu_{2-x}P_2$ [39], $SrCu_{2-x}P_2$ [39], $UNi_{2-x}P_2$ [16], $CeNi_{2-x}As_2$ [40], $CePd_{2-x}As_2$ [41], and a whole series of lanthanide-based $RENi_{2-x}Sb_2$, [42]. Qualitatively, this inherent non-stoichiometry can be explained through Zintl-like bonding considerations [43], noting that lower nickel, palladium or copper content would probably be favored since the fully stoichiometric RT_2X_2 would have too many valence electrons [44]. Thus, missing Ni atoms can be viewed as a result of the overall drive to optimize the Ni–P interactions in the structure—as briefly discussed above (and at length elsewhere [9]), reduced nickel content will not change much the population of the P–P bonding states, however, it will significantly reduce the population of the Ni–P anti-bonding states. Such deficiency on the transition metal sites is also common in the related $ZrCuSi_2$ type intermetallics [1], with the series $CeT_{1-x}Sb_2$ (T = Ni, Cu, Pd, Ag, Cd) [45–47] and $UT_{1-x}Sb_2$ compounds (T = Fe, Co, Ni, Cu, Ru, Pd, Ag and Au) [48–50] being just a few of the many examples.

3.2. Magnetism

Plots of the temperature dependence of the magnetic susceptibility ($\chi = M/H$) of three differently synthesized $PrNi_{2-x}P_2$ samples are displayed in Fig. 2. Above 50 K, the magnetic behavior follows the Curie–Weiss law $\chi = C/(T-\theta_P)$ [51], where $C = N_A\mu^2_{eff}/3k_B$ is the Curie constant and θ_P is the paramagnetic Weiss temperature. From the linear fits of the inverse susceptibility, the effective paramagnetic moments were calculated (from the data in the range 100–300 K), and the corresponding values are tabulated in Table 5. The moments in all cases are consistent with the magnetic behavior expected for trivalent Pr—the effective moment for free-ion Pr^{3+} according to the Hund's rules is $\mu_{eff} = 3.58\,\mu_B$ [51]. For the most heavily Ni-deficient specimen, we also observe a slight convex curvature of the $\chi^{-1}(T)$ dependence at low temperature (as presented in Supporting Information), leading to a negative Weiss constant.

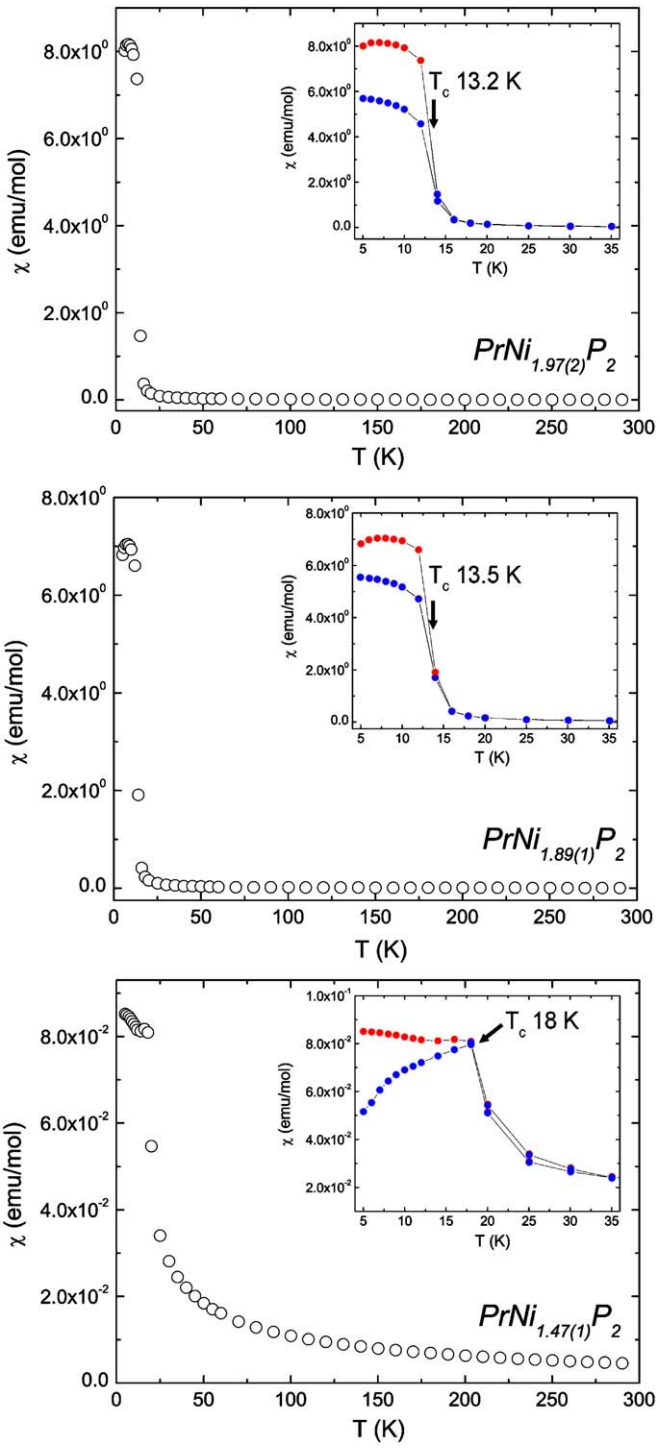

Fig. 2. Main panels: zero field-cooled magnetic susceptibility (χ) versus temperature of four different $PrNi_{2-x}P_2$ samples. Data are gathered at 500 Oe and normalized per mol. The insets show magnified views at low temperature of the field (red) and zero field-cooled (blue) magnetic susceptibility (χ) versus temperature. Data in this case are gathered at 100 Oe. All three samples were characterized by single-crystal X-ray diffraction and the formulas represent refined compositions. (For interpretation of references to colour in this figure legend, the reader is referred to the web version of this article.)

Table 5
Effective magnetic moments and ordering temperatures of $RENi_{2-x}P_2$ (RE = La, Ce, Pr).

Compound	Magnetic order[a]	μ_{eff} (μ_B)[b]	θ_p (K)	T_C (K)	Reference	Comment
$LaNi_2P_2$	none	Pauli paramagnetic			[52]	
$LaNi_{1.70(1)}P_2$	*none*	*Pauli paramagnetic*			*this work*	*No SC down to 5 K*
$CeNi_2P_2$	none	No Curie–Weiss behavior			[52]	
$CeNi_{1.72(1)}P_2$	*none*	*No Curie–Weiss behavior up to 300 K*			*this work*	*Kondo-like behavior*
$CeNi_{1.88(2)}P_2$	unknown	*No Curie–Weiss behavior up to 250 K*			*this work*	*possible AFM < 5 K*
$PrNi_2P_2$	FM	3.4	+12	n/a	[52]	T_C not reported
$PrNi_{1.97(2)}P_2$	*FM*	3.65	*+1.5*	*13.2*	*this work*	*T_C from $d\chi(T)/dT$*
$PrNi_{1.89(1)}P_2$	*FM*	3.59	*+3*	*13.5*	*this work*	*T_C from $d\chi(T)/dT$*
$PrNi_{1.47(1)}P_2$	*FM*	3.50	*−36*	*18*	*this work*	*possible FFM*

Results from this study are italicized.
[a] FM, AFM, FFM denote ferro-, antiferro- and ferri-magnetic interactions, respectively.
[b] Effective moments for free ion Ce^{3+} ($4f^1$) and Pr^{3+} ($4f^2$), according to the Hund's rules are 2.54 μ_B and 3.58 μ_B, respectively.

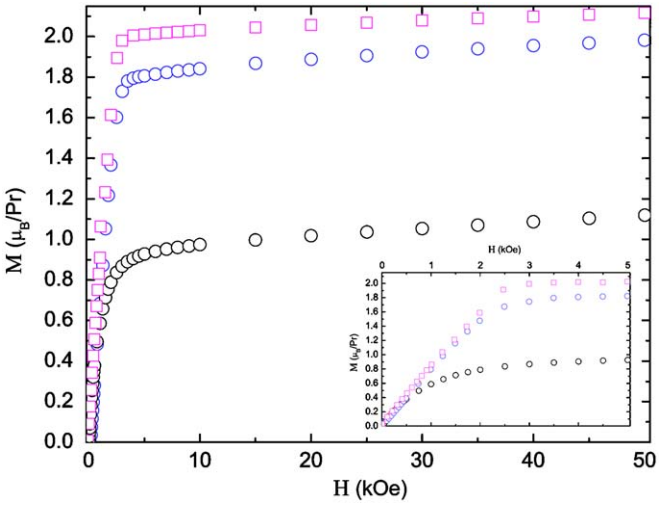

Fig. 3. Magnetization vs applied field for three different $PrNi_{2-x}P_2$ samples. Data are gathered at 5 K and normalized per Bohr-magneton (μ_B). The inset shows a magnified view at low field. Online color code: magenta—$PrNi_{1.97(2)}P_2$; blue—$PrNi_{1.89(1)}P_2$; black—$PrNi_{1.47(1)}P_2$. The saturation moments extrapolated to zero field in all cases are lower than the gJ value of 3.20 μ_B for Pr^{3+} [51] and decrease progressively as the Ni content decreases, suggesting a significant antiferromagnetic component to the ferromagnetically ordered structure.

The sharp increase of magnetic susceptibility of $PrNi_{1.97(2)}P_2$ and $PrNi_{1.89(1)}P_2$ below 30 K (reaching values of ca. 8 emu/mol and 7 emu/mol, respectively), together with the positive θ_P (Table 5) is suggestive of a transition to a ferromagnetic state. As the concentration of Ni-defects increases, for $PrNi_{1.47(1)}P_2$, the maximum susceptibility value decreases nearly 100-fold to about 0.08 emu/mol. Another evidence for the reduction of the effective magnetic moment of Pr^{3+} in $PrNi_{1.47(1)}P_2$ is represented in Fig. 3, where the magnetization isotherms for $PrNi_{2-x}P_2$ are displayed, all taken at 5 K. As clearly seen from the data, the saturation moments extrapolated to zero field are lower than gJ [51] and decrease progressively as the Ni content decreases. These observations, alongside the calculated negative Weiss constants for the latter sample, seem to indicate that anti-ferromagnetic fluctuations are also present and strongly influence the nature of the long-range order as the number of Ni defects increases. An interplay of locally inequivalent Pr sites in the defect-rich samples (allowing for a possible ferrimagnetic ground state) and crystalline field (CEF) effects can also be suggested as the origin for this behavior.

An inspection of the low temperature $\chi(T)$ curves for the $PrNi_{2-x}P_2$ samples, measured at very weak applied fields provides another evidence for a complex magnetism. As seen from the insets of Fig. 2, field and zero-field measurements reveal disparities in the magnetic susceptibility, which are indicative of the onset of long-range ferromagnetic order. The corresponding ordering temperatures were determined from the mid-point in the jump in $d\chi/dT$, and show that the transition temperature increases with increased concentration of Ni-defects. Such variations are not surprising, given that the magnetic order in intermetallics with the $ThCr_2Si_2$ type is known to be very sensitive to the c/a ratio [2]. In very simplistic terms, one might consider it as an artifact of the number of electrons in conduction bands. If this reckoning holds true for the discussed $PrNi_{2-x}P_2$ samples, the apparent trend is that higher Ni-deficiency leads to a lower valence electron concentration (Table 1—c/a ratio decreases), thereby, higher Curie temperatures. In the context of this reasoning, we also recall that the maximum susceptibility values change 2 orders of magnitude on going from nearly stoichiometric $PrNi_{1.97(1)}P_2$ to a defect-rich $PrNi_{1.47(1)}P_2$, which may suggest the proximity of a (chemical) pressure induced phase transition. Ultimately, neutron or synchrotron diffraction experiments at lower temperature and/or under pressure are needed in order to provide a better explanation.

Plots of the magnetic susceptibility and the inverse susceptibility of two $CeNi_{2-x}P_2$ samples as a function of the temperature are displayed in Fig. 4. From the $\chi(T)$ and $\chi^{-1}(T)$ dependence of $CeNi_{1.72(1)}P_2$, it is clear that the magnetic susceptibility does not follow the Curie–Weiss law; instead, it shows the characteristics of a mixed valent Ce^{3+}/Ce^{4+} system. Similar $c(T)$ dependence is seen for another $CeNi_{2-x}P_2$ batch, having much fewer Ni-defects (Table 1). The data for $CeNi_{1.88(2)}P_2$ also reveal a possible antiferromagnetic ordering transition below 5 K (judged from the order of magnitude higher maximum susceptibility value). Jeitschko and Reehuis also mention the lack of a typical Ce^{3+} local-moment magnetism for a reportedly stoichiometric $CeNi_2P_2$ [52]. Another corroborating evidence for Ce^{4+} can be found in the structural data too—the unit cell volumes of $CeNi_{1.88(1)}P_2$ and $PrNi_{1.89(1)}P_2$ are the same (Table 1)—an obvious discrepancy with the lanthanide contraction, which is due to the smaller size of Ce^{4+} vs Ce^{3+}. Based on the above, and taking into account the fact that the M vs H isotherm for $CeNi_{1.72(1)}P_2$ (Fig. 5) shows a very low moment and no tendency for saturation in fields up the 50 kOe, it appears that such mixed-valent behavior is intrinsic to all $CeNi_{2-x}P_2$ specimens.

The magnetizations of two different $LaNi_{2-x}P_2$ samples ($x \approx 0.3$) were measured in an applied field of 100 Oe. The data (not shown) indicate very weak and virtually temperature-independent paramagnetism (a slight upturn was seen at low temperature, but it is most likely due to a small paramagnetic impurity). This is consistent with the Pauli-like behavior expected for La^{3+}

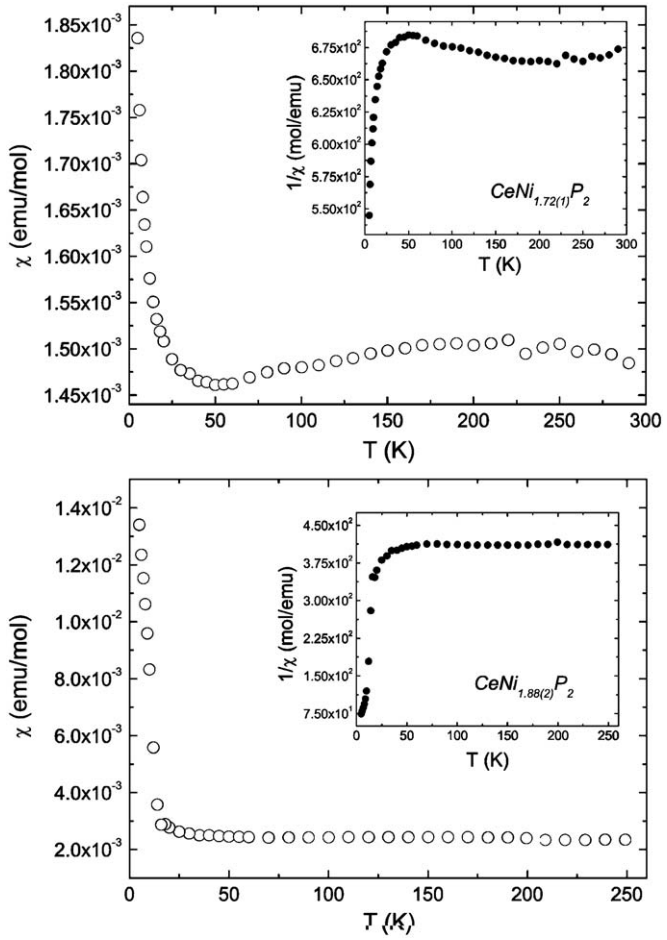

Fig. 4. Main panels: zero field-cooled magnetic susceptibility (χ) versus temperature of $CeNi_{1.72(1)}P_2$ and $CeNi_{1.88(2)}P_2$. Data are gathered at 500 Oe and normalized per mol. The inset shows the inverse magnetic susceptibility as a function of temperature.

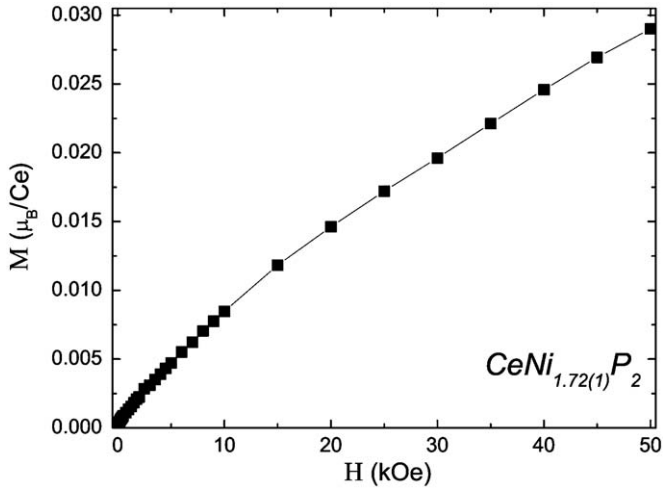

Fig. 5. Magnetization vs applied field for $CeNi_{1.72(1)}P_2$. Data are gathered at 5 K and shown in Bohr-magneton units. The saturation moments extrapolated to zero field is two orders of magnitude lower than the *gJ* value of 2.14 μ_B expected for Ce^{3+} [51], confirming the mixed valent state.

(closed-shell) and the data for the isotypic $CaNi_2P_2$ [52]. There was no evidence for a superconducting transition down to 5 K.

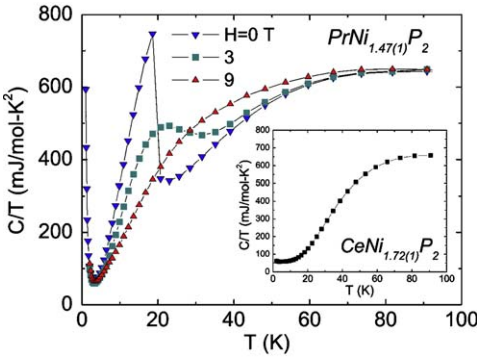

Fig. 6. Main panel: Specific heat of $PrNi_{1.47(1)}P_2$ versus temperature at zero field and at applied field of 30 and 90 kOe, respectively. Data are represented in the form $C_p(T)/T$ vs T to clearly show the anomaly due to the magnetic ordering transition. The inset shows the specific heat of $CeNi_{1.72(1)}P_2$ versus temperature at zero field in the same representation.

3.3. Heat Capacity

To further study the magnetic ground state in $CeNi_{1.72(1)}P_2$ and the nature of the magnetic order in $PrNi_{1.47(1)}P_2$, heat-capacity measurements were carried out in fields up to 90 kOe. The specific heat C vs temperature plots for these samples are shown in Fig. 6, plotted in the representation C/T vs T. An anomaly corresponding to the magnetic transition in $PrNi_{1.47(1)}P_2$ is clearly seen at $TC \approx 18$ K; it broadens considerably and moves up in temperature with increasing the field ($TC \approx 27$ K at $H = 30$ kOe). With the applied field further increased to 90 kOe, the peak eventually disappears. Such field-dependence of the heat-capacity is characteristic of a ferromagnetic ordering. A nuclear Schottky anomaly due to the Pr^{3+} ions is also observed at the lowest temperatures, making estimates of the electronic and phonon contributions to the specific heat difficult.

The mixed valent behavior in $CeNi_{1.72(1)}P_2$, which was suggested above on the basis of the $\chi(T)$ dependence is corroborated in the heat capacity (Fig. 6—inset). The lack of a magnetic ordering in this case was confirmed down to 2 K. From the linear fit of C/T vs T^2 at low temperature, a Sommerfeld coefficient $\gamma \approx 60$ mJ/mol K^2 was extracted. Its low value, taken together with the broad maximum in the susceptibility and no tendency for saturation in applied magnetic fields is suggestive of a fully degenerate Ce ground state with a spin fluctuation temperature above room temperature.

4. Conclusions

With the present work, the previously known as the line compounds $RENi_2P_2$ (RE = La, Ce, Pr) were reexamined. Based on structure refinements and data from property measurements, the title compounds were hereby reformulated as non-stoichiometric, Ni-deficient $RENi_{2-x}P_2$ phases, whose structure accommodates a wide range of defects on the transition metal site. This study also proved a strong dependence between the phase widths and the reaction temperatures. The small changes in the Ni-underoccupancy were shown to ultimately affect the magnetism of the synthesized materials, emphasizing once again the importance of the diligence and care in synthesis and structural characterization for understanding the properties of a given material. Since the $\chi(T)$ data for $CeNi_{1.72(1)}P_2$ are reminiscent with the characteristics of a Kondo-system (with a temperature scale on the order of 1000 K ($T_K \approx 4 \times T^{\chi}_{max}$), currently, attempts to study and fully characterize a series of $CeNi_{2-x}P_2$ samples are under way.

Acknowledgments

Svilen Bobev gratefully acknowledges funding from the University of Delaware through start-up funds. Work at LANL was performed under the auspices of the US DOE, Office of Science. The authors also thank Mr. Benjamin Hmiel for synthesizing some of the samples and Mr. Bayrammurad Saparov for his assistance with the SQUID measurements.

Appendix A. Suppmentary data

Supplementary data associated with this article (indexed powder X-ray diffraction pattern of $PrNi_{1.47(2)}P_2$, as well as the non-linear fit of the $\chi(T)$ data for $PrNi1.47(1)P_2$ and the corresponding linear fit of the $\chi^{-1}(T)$ can be found in the online version at doi:10.1016/j.jssc.2009.03.014.

References

[1] P. Villars, L.D. Calvert (Eds.), Pearson's Handbook of Crystallographic Data for Intermetallic Compounds, second ed., American Society for Metals, Materials Park, OH, USA, 1991 and the desktop edition 1997.
[2] A. Szytula, J. Leciejewicz, in: Handbook of Crystal Structures and Magnetic Properties of Rare Earth Intermetallics, CRC Press, Boca Raton, FL, 1994.
[3] E. Parthé, B. Chabot, H.F. Braun, N. Engel, Acta Crystallogr. B 39 (1983) 588.
[4] W.B. Pearson, J. Solid State Chem. 56 (1985) 278.
[5] R. Hoffmann, C. Zheng, J. Phys. Chem. 89 (1985) 4175.
[6] C. Zheng, R. Hoffmann, R. Nesper, H.-G. von Schnering, J. Am. Chem. Soc. 108 (1986) 1876.
[7] C. Zheng, R. Hoffmann, J. Solid State Chem. 72 (1988) 58.
[8] J.K. Burdett, G.J. Miller, Chem. Mater. 2 (1990) 12.
[9] D. Johrendt, C. Felser, O. Jepsen, O.K. Andersen, A. Mewis, J. Rouxel, J. Solid State Chem. 130 (1997) 254.
[10] U. Haussermann, S. Amerioun, L. Eriksson, C.-S. Lee, G.J. Miller, J. Am. Chem. Soc. 124 (2001) 4371.
[11] F. Steglich, J. Aarts, C.D. Bredl, W. Lieke, D. Meschede, W. Franz, H. Schäfer, Phys. Rev. Lett. 43 (1979) 1892.
[12] I. Felner, I. Nowik, Solid State Commun. 47 (1983) 831.
[13] C. Broholm, J.K. Kjems, W.J.L. Buyers, P. Matthewes, T.T.M. Palstra, A.A. Menovsky, J.A. Mydosh, Phys. Rev. Lett. 58 (1987) 1467.
[14] W. Jeitschko, R. Glaum, L. Boonk, J. Solid State Chem. 69 (1987) 93.
[15] R. Marchand, W. Jeitschko, J. Solid State Chem. 24 (1978) 351.
[16] T. Ebel, W. Jeitschko, J. Solid State Chem. 116 (1995) 307.
[17] P.G. Pagliuso, J.L. Sarrao, J.D. Thompson, M.F. Hundley, M.S. Sercheli, R.R. Urbano, C. Rettori, Z. Fisk, S.B. Oseroff, Phys. Rev. B 63 (2001) 092406.
[18] I. Nowik, I. Felner, C. Mermelstein, E.R. Bauminger, Hyperfine Interact. 54 (1990) 847.
[19] B. Li, J.D. Corbett, Inorg. Chem. 46 (2007) 8812.
[20] F. Ahmadpour, T. Kolodiazhnyi, Y. Mozharivskyj, J. Solid State Chem. 180 (2007) 2420.
[21] A.V. Tkachuk, A. Mar, J. Solid State Chem. 180 (2007) 2298.
[22] A.S. Sefat, R. Jin, M.A. McGuire, B.C. Sales, D.J. Singh, D. Mandrus, Phys. Rev. Lett. 101 (2008) 117004.
[23] N. Ni, S.L. Bud'ko, A. Kreyssig, S. Nandi, G.E. Rustan, A.I. Goldman, S. Gupta, J.D. Corbett, A. Kracher, P.C. Canfield, Phys. Rev. B 79 (2008) 14507.
[24] M. Rotter, M. Tegel, D. Johrendt, Phys. Rev. Lett. 101 (2008) 107006.
[25] M. Rotter, M. Tegel, D. Johrendt, Angew. Chem. Int. Ed. 47 (2008) 7949.
[26] S. Bobev, E.D. Bauer, J.D. Thompson, J.L. Sarrao, J. Magn. Magn. Mater. 277 (2004) 236.
[27] S.Q. Xia, P. King, S. Bobev, Acta Cryst. E 62 (2006) i184.
[28] P.H. Tobash, S. Bobev, J. Alloys Compd. 418 (2006) 58.
[29] S. Bobev, J. Merz, A. Lima, V. Fritsch, J.D. Thompson, J.L. Sarrao, M. Gillessen, R. Dronskowski, Inorg. Chem. 45 (2006) 4047.
[30] S.-Q. Xia, C. Myers, S. Bobev, Eur. J. Inorg. Chem. (2008) 4262.
[31] Y. Kamihara, T. Watanabe, M. Hirano, H. Hosono, J. Am. Chem. Soc. 130 (2008) 3296.
[32] W. Jeitschko, B. Jaberg, J. Solid State Chem. 35 (1980) 312.
[33] W.K. Hofmann, W. Jeitschko, J. Solid State Chem. 51 (1984) 152.
[34] M.G. Kanatzidis, R. Pöttgen, W. Jeitschko, Angew. Chem. Int. Ed. 44 (2005) 6996.
[35] JADE Version 6.5, Materials Data, Inc., Livermore, CA 2003.
[36] Bruker *SMART* and *SAINT*, Bruker AXS Inc., Madison, Wisconsin, USA, 2002.
[37] G.M. Sheldrick, SADABS, University of Göttingen, Germany, 2003.
[38] G.M. Sheldrick, SHELXTL, University of Göttingen, Germany, 2001.
[39] A. Mewis, Z. Naturforsch. B 354 (1980) 141.
[40] E.H. El Ghadraoui, J.Y. Pivan, R. Guérin, O. Pena, J. Padiou, M. Sergent, Mat. Res. Bull. 23 (1988) 1345.
[41] P. Quebe, W. Jeitschko, J. Solid State Chem. 115 (1995) 37.
[42] W.K. Hofmann, W. Jeitschko, J. Less-Common Met. 138 (1988) 313.
[43] For the discussed nickel-phosphides, if stoichiometric, this means a zero formal charge on the $[Ni_2P_2]^0$ framework, i.e., *RE*Ni_2P_2 will be electron-rich assuming a nominally trivalent *RE* cation. The same reasoning rebuffs the hypothesis of mixing Ni and P at the 4*d* site, as the formula $RENi_{2-x}P_{2+x}$ will be even electron-richer.
[44] Along the same line of thinking, it is easy to explain why the vast majority of compounds in this family are transition-metal silicides and germandides with the alkaline-earth and rare-earth cations—they are formally 14 and 15 electron species, respectively, and they are largely defect-free [2].
[45] Y. Muro, N. Takeda, M. Ishikawa, J. Alloys Compd. 257 (1997) 23.
[46] A.V. Tkachuk, A. Mar, Acta Crystallogr. E 60 (2004) i82.
[47] P.H. Tobash, S. Bobev, Acta Crystallogr. E 61 (2005) i174.
[48] D. Kaczorowski, R. Kruk, J.P. Sanchez, B. Malaman, F. Wastin, Phys. Rev. B 58 (1998) 9227.
[49] S. Bobev, D.J. Mixson, E.D. Bauer, J.L. Sarrao, Acta Crystallogr. E 62 (2006) i64.
[50] S. Bobev, D.J. Mixson, E.D. Bauer, J.L. Sarrao, Acta Crystallogr. E 62 (2006) i66.
[51] J.S. Smart, Effective Field Theories of Magnetism, Saunders, Philadelphia, PA, 1966.
[52] W. Jeitschko, M. Reehuis, J. Phys. Chem. Solids 48 (1987) 667.